



Article

Investigation on Surface Roughness of PolyJet-Printed Airfoil Geometries for Small UAV Applications

Orhan Gülcan *, Kadir Günaydın * and Alican Çelik

General Electric Aviation, Additive Design, Kocaeli 41400, Turkey; alican.celik@ge.com

* Correspondence: orhan.gulcan@ge.com (O.G.); kadir.gunaydin@ge.com (K.G.); Tel.: +90-262-677-8410 (O.G.)

Abstract: The present study focuses on producibility and surface roughness characteristics of airfoil geometries and their effect on aerodynamic performance for different velocities, surface roughness values and angles of attack. Two different tray orientations (along X and Y axis), two different build directions (vertical and horizontal) and two different surface finish settings (matte and glossy) were used to evaluate the effect of these parameters on the surface roughness of both up- and down-facing surfaces of airfoils produced by PolyJet. On both surfaces, surface roughness measurements were performed on two crossing directions. The results showed that horizontal build direction where surfaces of airfoils were parallel to the build platform experienced lower surface roughness than the vertical build direction. Vertically oriented specimens showed a considerable degree of distortions especially in trailing edges along with very high surface irregularities on side walls. In general, glossy or matte finish settings resulted in similar surface roughness values and specimens located along X direction showed better surface quality than specimens located along Y direction with an inconsiderable difference. Besides this, CFD analysis revealed that surface roughness caused by printing strategies directly influences the aerodynamic performance of the fixed-wing UAVs (Unmanned Aerial Vehicles) to considerable degrees. The increase in the drag force coefficient, due to surface roughness, reached almost 7.5% for high cruise velocity at 0° angle of attack and 13% at 10° angle of attack in which stall commences.

Keywords: airfoil; aerodynamic performance; PolyJet; surface roughness; tray location; build direction; surface finish setting; glossy; matte



Citation: Gülcan, O.; Günaydın, K.; Çelik, A. Investigation on Surface Roughness of PolyJet-Printed Airfoil Geometries for Small UAV Applications. *Aerospace* **2022**, *9*, 82. <https://doi.org/10.3390/aerospace9020082>

Academic Editor: Chiara Bisagni

Received: 13 December 2021

Accepted: 28 January 2022

Published: 3 February 2022

Publisher's Note: MDPI stays neutral with regard to jurisdictional claims in published maps and institutional affiliations.



Copyright: © 2022 by the authors. Licensee MDPI, Basel, Switzerland. This article is an open access article distributed under the terms and conditions of the Creative Commons Attribution (CC BY) license (<https://creativecommons.org/licenses/by/4.0/>).

1. Introduction

Unmanned aerial vehicles (UAV) are flying robots that fly remotely or autonomously without carrying a human operator [1]. UAVs can be small or large in size for their specific purposes. Among different UAVs, especially small or mini UAVs, they find their usage in different industries and applications (search and rescue operations, security and surveillance purposes, air pollution detection, road traffic monitoring, delivery of goods, agriculture, photogrammetry and remote sensing purposes, etc.) due to their low cost and simplicity of operation [2–4]. These small UAVs can be classified via different aspects. P.S. and Jeyan reviewed the classifications of small UAVs in terms of operating altitude, endurance, operating range, maximum take of weight and payload. Their review revealed that an average operating range of 30–40 km, an average operating altitude of 3500 m, an average endurance of 3–4 h and an average maximum takeoff weight of 30 kg can be used as working parameters in UAV applications based on the literature [5].

Different materials (composite materials such as fiberglass, Kevlar, fiber carbon, etc. and other materials such as Styrofoam, wood, plastics, etc.) and production techniques have been used for small UAV production up to now [6]. With the advancements in the technology, additive manufacturing (AM) methods have also been applied to production of small UAVs.

AM is based on layer-by-layer manufacturing and unlike conventional manufacturing techniques it has a very low buy-to-fly ratio [7]. Different AM methods (powder-bed fusion, directed energy deposition, binder jetting, material jetting, material extrusion, sheet lamination, and vat photopolymerization) can be used for different applications [8]. Among these methods, PolyJet technology has a very wide area of applications for polymeric materials [9]. PolyJet technology is another name for material jetting process in which photopolymer materials are deposited on a build platform as droplets forming a very thin layer [10] and ultraviolet (UV) light is used to cure the material on the build platform [11], as seen in Figure 1. After curing a layer, the build platform is lowered with an amount of layer thickness and the process continues by jetting new liquid material onto the previous layer. When all the layers are successively cured, a full-scale part is obtained [12]. Since the material used in PolyJet is in a liquid state, a support structure is needed especially in overhanging regions and these support structures need to be removed from the part after printing [13].

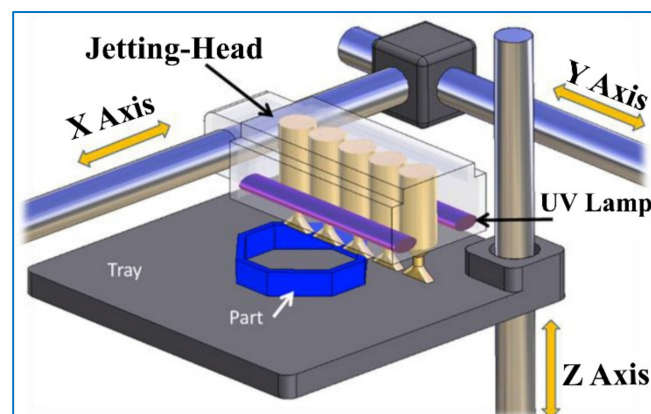


Figure 1. PolyJet technology with three moving axes. Adapted from [9].

In most of the studies performed in the literature, it was stated that high surface quality parts are obtained with PolyJet technology. However, this quality or amount of surface roughness depends on different geometrical and process parameters. Tray location, build orientation, layer thickness, type of material, surface finish setting and post processing are some of the parameters that affect the surface roughness of PolyJet-printed parts [14,15].

The effectiveness of these parameters on the surface roughness of PolyJet-printed parts has been investigated in the literature. Kechagias et al. stated that lower layer thickness (16 μm) and glossy surface finish setting resulted in lower surface roughness values and scale factor was not a dominant factor on surface roughness [16]. Aslani et al. stated that surface finish setting (matte or glossy) has the highest effect on surface roughness with a contribution rate of 95%. On the other hand, layer thickness and build scale have very little effect on surface roughness with a contribution rate of less than 3% [17].

Locating the part along the X or Y axis of the build tray in PolyJet has some amount of effect on the surface roughness of the final parts. Cazon et al. stated that the best roughness results were obtained when the parts were placed close to the XY plane [15]. Beltrán et al. stated that part orientation and part size have the main influence and part location on build plate has a relatively lower influence on quality of PolyJet-printed parts [18].

The build orientation of parts with respect to build tray also affects the surface roughness of PolyJet-printed parts. Kumar and Kumar stated that the surface roughness is generally increased with an increase in build orientation up to 90° in PolyJet-printed parts [19]. In another study, the same authors stated that the build orientation and surface finish setting were the major factors affecting surface roughness and maximum surface roughness was obtained for the 90° build orientation [20]. Similar results were observed in Kechagias and Stavropoulos' study where they stated that surface roughness increased with an increase in the angle of sloped surfaces and the best and worst values of surface

roughness were observed when the angle of sloped surfaces was 0 and 90°, respectively [21]. Khoshkhoo et al. suggested using tiltable build platforms and printing parameters such as localized build orientation, build orientation and selective support structures to obtain high quality surfaces [22]. In their experimental study, Vidakis et al. stated that parts produced in X direction showed lower surface roughness when the sloped surface angle was below 45°; after that value, parts produced in Y direction had lower surface roughness values [23]. Kent et al.'s study revealed that build orientation has a very high impact on dimensional accuracy and surface roughness of PolyJet-printed parts [24].

In PolyJet technology, two printing modes are used: high speed and high quality (with low layer thickness). Related with support strategy, matte and glossy surface finish options are used in PolyJet technology where the whole part is covered with support material in the matte setting and only structurally needed areas are supported in the glossy setting [25]. Pugalendhi et al. stated that the glossy finish option resulted in lower peaks and valleys and therefore lower surface roughness than matte finish options [26]. A similar result was found by Cazon et al. [15]. This lower surface roughness with the glossy surface finish option resulted in a higher fatigue life, as stated by Moore et al. [27].

Related to UAV applications, fused deposition manufacturing (FDM) was used for individual component or full-scale part production [28] but since PolyJet technology offers higher surface-quality parts with higher dimensional accuracy than FDM as stated in different studies [29–37], the application of PolyJet in the UAV industry increases day by day. PolyJet has been used to rapidly manufacture and test various wing prototype designs [12] and to produce wing structures with different types of lattice designs to achieve a light weight [38]. The performance of small UAVs in different applications is affected by size, power, speed, payload, etc. [39].

The surface roughness characteristics of air flow-impacted areas (i.e., wing surfaces) are directly related to the performance of UAVs. Airfoils and airfoil-like geometries are a very important part of the aviation industry and the surface roughness of these geometries directly affects aerodynamic performance. To the best of the authors' knowledge, the available scientific literature has a gap for PolyJet-printed airfoil geometries and their surface roughness characteristics and performance. To fill this gap, this study focuses on producibility and surface roughness of airfoil geometries in PolyJet. Two different tray orientations (X and Y direction), two different build directions (horizontal and vertical) and two different surface finish settings (matte and glossy) were used to investigate the effect of these parameters on producibility and surface roughness. To evaluate the surface roughness values, contact-type profilometer was utilized to obtain the arithmetic average roughness. Then, for elucidating the effect of surface roughness on aerodynamic performance of fixed-wing UAVs, CFD analyses were performed with different inlet velocities, angles of attack and measured surface roughness values.

The rest of the paper is organized as follows. Section 2 describes the production parameters, material details, surface roughness measurement details and numerical analysis methodology. Section 3 introduces surface roughness measurements and numerical analysis results. In Section 4, results presented in Section 3 are discussed in terms of tray location, build orientation, surface finish settings, and effect of build configuration on aerodynamic performance.

2. Materials and Methods

2.1. Production and Surface Roughness

Airfoil geometry (NACA0008) to be printed by PolyJet was modelled using NX 12 CAD software (Siemens AG, Munich, Germany). Figure 2 shows CAD geometry with main dimensions. CAD geometry was converted into stl format and build layout was prepared by orienting the specimens along X and Y directions with two build orientations (horizontal and vertical) (Figure 3). Specimens were printed in Stratasys Objet Connex1 PolyJet machine (Stratasys Ltd., Rehovot, Israel) with two different surface finish options (matte or glossy) (Table 1). High quality printing mode with 16 µm layer thickness was used to obtain better

surface finish results. Transparent RGD720 material (Stratasys Ltd., Rehovot, Israel) was used as the main material and solution soluble SUP706B material (Stratasys Ltd., Rehovot, Israel) was used as support material. Both matte and glossy surface finish options were used in the experiments. After printing airfoil geometries, support structures were removed from the specimens with sodium hydroxide (NaOH) solution. All surface roughness measurements were performed with a contact (stylus)-type profilometer (Mitutoyo SJ-400 roughness measurement device (Mitutoyo Ltd., Andover, Hampshire, UK)). For vertically oriented samples, surface roughness measurements were performed on two side surfaces and at three locations along the X, Y and Z axes. On the other hand, for horizontally oriented samples, surface roughness measurements were performed on two side surfaces (up facing and down facing) and at three locations along the X and Y axes. The average of three surface roughness measurement results were used in evaluations.

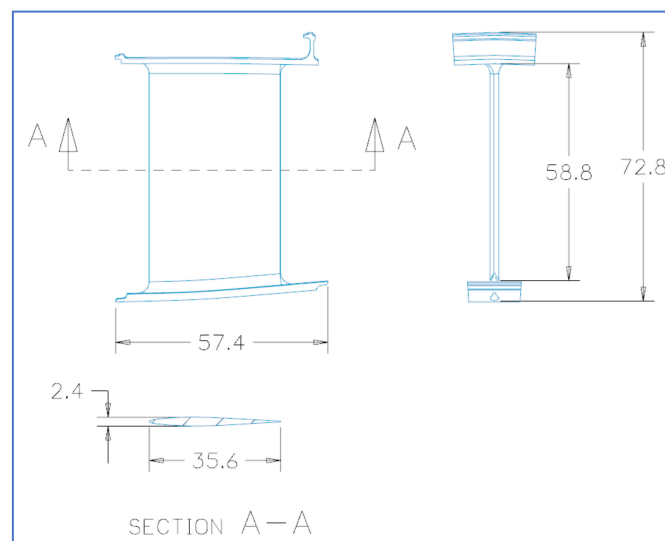


Figure 2. General dimensions of airfoil geometry. Dimensions are in mm.

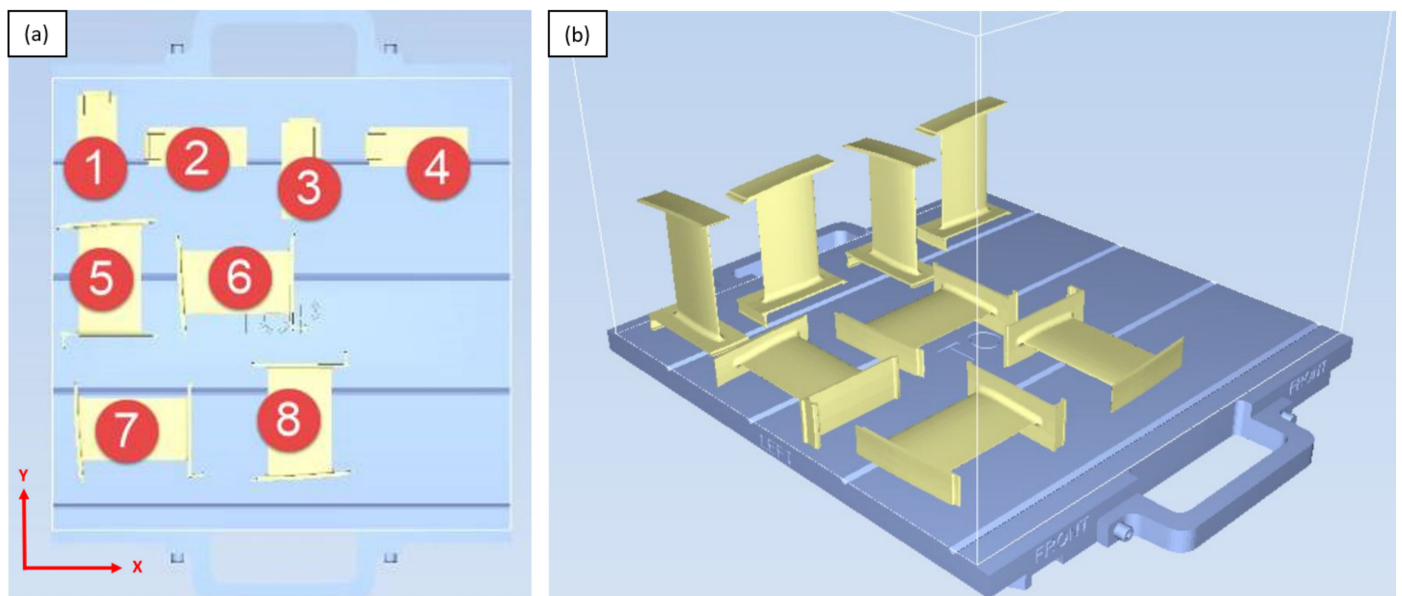


Figure 3. (a) Build layout looking from above; (b) build layout in isometric view.

Table 1. Tray location, build orientation and surface finish settings of specimens.

Specimen #	Tray Location	Build Orientation	Surface Finish Setting
1	Along Y axis	Vertical	Matte
2	Along X axis	Vertical	Matte
3	Along Y axis	Vertical	Glossy
4	Along X axis	Vertical	Glossy
5	Along Y axis	Horizontal	Matte
6	Along X axis	Horizontal	Matte
7	Along X axis	Horizontal	Glossy
8	Along Y axis	Horizontal	Glossy

2.2. Numerical Analysis

Considering serious requirements for miniature fixed-wing UAVs during landing, take-off or cruise, improved strength and stability are needed. The wings of the UAVs bear severe bending and twisting loads during flight, and these loads make fixed-wings prioritized for UAV designs. Moreover, any irregular shape of the wings or high surface roughness decreases the aerodynamic performance of the UAV wings and reduces cruise duration due to limited stored energy. Thus, to define the structural robustness of the fixed-wing UAVs and their performance, experimental analyses are required. However, due to demanding testing equipment for evaluating the performance and requirements of wings such as full-scale wind tunnels and vibration testing machines, the conformity of UAVs is investigated using numerical tools [40]. In this study, the aerodynamic analysis of the wing of a miniature fixed-wing UAV that was designed with NX12 CAD software was conducted with ANSYS Fluent[®] software (Ansys, Canonsburg, PA, USA).

Forces acting on a structure moving in a fluid are caused by pressure distribution and shear stress over the surface of the structure. Two types of explicit main forces are generated during the moving in a fluid, which can be listed as drag and lift forces. Lift (L) is one of the aerodynamic force components that emerge in the perpendicular direction of the flow, and another aerodynamic force component is the drag force (D), which occurs along the flow direction. To characterize and calculate the effect of flow on the immersed structure in the fluid, dimensionless parameters are derived from the abovementioned forces. Furthermore, in the fundamental design and performance studies of airplanes and fixed-wing UAVs, lift and drag coefficients play a significant role. The lift coefficient, C_L , is a dimensionless coefficient that is derived for defining the relation with the lifted body (foil or a full body such as fixed-wing aircraft) and surrounded fluid, and it is related to fluid density around the body, the velocity of surrounded fluid and the reference area of body. In other words, lift coefficient varies as a function of Reynolds number (Re), Mach number and the angle of the body to the surrounded fluid flow direction. Another fundamental dimensionless quantity that is used to define the amount of drag force is drag coefficient, C_D . The impacts of the two primary contributions to fluid dynamic drag—skin friction and form drag—are combined in the drag coefficient of any object. The drag coefficient is a function of body size, fluid velocity, fluid density and fluid viscosity. It also varies as a function of Reynolds number, Mach number and the angle of the body in the fluid [41].

The lift C_L and drag C_D are defined as:

$$C_L = \frac{L}{\frac{1}{2}\rho_{\infty}V_{\infty}^2S} \quad (1)$$

$$C_D = \frac{D}{\frac{1}{2}\rho_{\infty}V_{\infty}^2S} \quad (2)$$

In these equations, ρ_{∞} and V_{∞} are defined as the freestream density and velocity, respectively. S is the reference area, in other words, it is the nominal wing area [41]. Moreover, some additional parameters are utilized for characterizing fixed-wing airfoil geometry such as mean aerodynamic chord (MAC) which is the distance between the

leading and trailing edge of the wing. Moreover, the type of the flow is important for the analysis, and the Reynolds number denotes whether the flow is laminar or turbulent, and the transition Reynolds number for defining the characteristic of flow is called critical Reynolds number [41,42]. Reynolds number is denoted by the density of the fluid, flow speed, characteristic linear dimension and dynamic viscosity of the fluid. All of these parameters used in the analysis are listed in Table 2.

Table 2. UAV velocity characteristics.

Low Velocity	Mid-Level Velocity	High Velocity
40 km/h	65 km/h	90 km/h

For the numerical analysis, the fluid inlet velocity needs to be defined; thus, the velocity of different small fixed-wing miniature UAVs in the market were surveyed. The fixed-wing miniature UAVs in the market experience different velocities. For instance, the UAV used for image acquisition experiences 40 km/h velocity [43]. Chmielewski and Sibilski studied developing an optics-based system to measure the ground velocity of the UAV, and X-UAV Talon EPO was utilized in this study, which exhibited 75 km/h velocity [44]. Mittal and Muneshwar projected the design and development of a miniature UAV called Sparrow S that reaches cruise velocity of 80–90 km/h [45]. The velocities achieved by other miniature UAVs are listed as 70 km/h [46], 70–90 km/h [47], 75 km/h and 72 km/h [48]. According to the velocities of the UAVs in the literature and in the market, three different velocities were selected to categorize the velocity of fixed-wing UAVs in three groups: 90 km/h, 65 km/h and 40 km/h for high-velocity UAVs, mid-level velocity UAVs and low-velocity UAVs, respectively, as displayed in Table 2. According to the defined velocities, the calculated Reynolds number for low velocity, mid-level velocity and high velocity are 2.71×10^4 , 4.40×10^4 and 6.09×10^4 , respectively. The critical Reynolds number varies from 1×10^5 to 3×10^6 for flows across a flat plate and it is in the range of Siemens AG 1×10^3 to 2×10^5 for airfoil profiles which is strongly based on the maximum thickness of the airfoil profile [42]. Moreover, these three types of velocities were utilized as a free-stream inlet velocity in the analyses for a 0° angle of attack. Besides, the angle of attack of the fixed-wing was selected in the range of -5° to 30° with an interval of 5° to determine the effect of surface roughness on drag and lift coefficients values in different angles of attack for the high-velocity UAVs.

In the analysis, a fluid domain of a $300 \times 200 \times 50$ mm cuboid was exploited and the chord point on the leading edge of the fixed-wing model was placed at the origin of the cuboid. In addition, another cuboid is located at the trailing edge of the wing in order to refine the mesh in the vicinity and downstream of the model for capturing characteristics of the wake. The boundary condition of velocity inlet is defined in the front part of the cuboid as a surface and a pressure outlet was at the backside of the cuboid with atmospheric conditions. Symmetry boundary conditions was applied at both the up- and downside of the cuboid. The data in Table 3 is used for the analysis.

Table 3. Analysis parameters.

MAC	Wing Area	Viscosity	Density
35.6 mm	3500 mm ²	1.7894×10^{-5} kg/m.s	1.225 kg/m ³

The flow type was determined as turbulent flow according to the Reynolds number; thus, a convenient turbulence model should be determined to monitor the effect of the flow on the wing and the effect of surface roughness. Ansys® Documentation suggests Realizable $k-\epsilon$ or SST $k-\omega$ turbulence models for the analysis of standard cases in which surface roughness effects are also taken into account [49]. Sadikin et al. indicated that SST $k-\omega$ model provides better results in comparison to Realizable $k-\epsilon$ model in the study of

comparative turbulence models on aerodynamic characteristics of a NACA0012 airfoil for high Reynolds number flow (3×10^6) [50]. Thus, SST $k-\omega$ turbulence model is selected for the CFD analysis. As for meshing, a polyhedral mesh was used instead of the conventional tetrahedral mesh type, and a mesh convergence study was conducted to define the mesh size. The number of divisions for meshing in the perpendicular direction of the wing is 210 and 310 on the later side. A 0.1 mm mesh size was used for the cuboid located at the trailing edge of the wing in order to refine the mesh in the vicinity and downstream of the model, as seen in Figure 4.

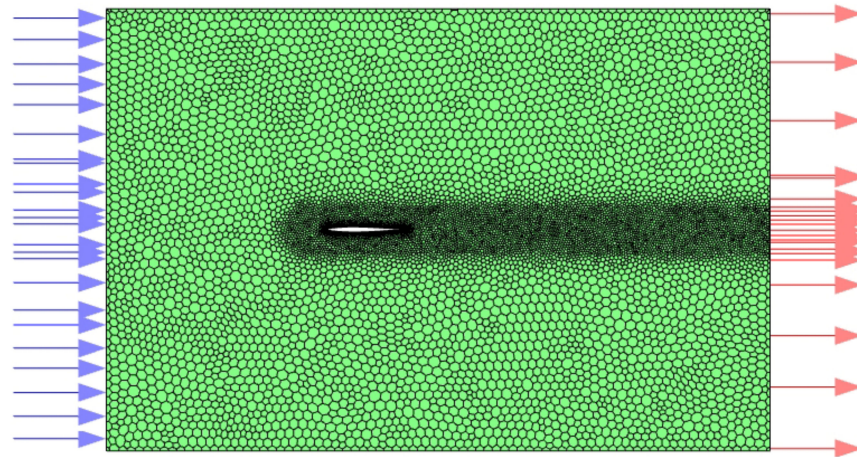


Figure 4. Polyhedral meshed computational fluid dynamic model.

To model the surface roughness for the flow analysis, two roughness parameters need to be specified. The first one is the Roughness Constant (C_s), the default value of which is 0.5 and denotes uniform roughness. For non-uniform roughness types, a higher value between 0.5 and 1.0 is more convenient to demonstrate the effect of surface roughness. In this study, the roughness constant is accepted as 0.5 according to surface roughness measurement results. Another parameter is the roughness height (K_s), the default value of which is zero, and denotes the smooth walls. For experiencing the effect of surface roughness, the value of roughness height needs to be greater than zero [49]. Some methods are utilized for calculating the roughness height; however, some studies show that the arithmetical mean deviation (R_a) of the assessed profile has a correlation with roughness height [51–54]. In this analysis, a $K_s/R_a = 5.2$ ratio is utilized to calculate the roughness height from the arithmetical mean deviation roughness value [55]. The surface roughness measurements were broken down into three groups: smooth, mid-level roughness and high roughness. Thus, three different R_a values including smooth ($0 \mu\text{inch } R_a$), mid-level roughness ($88.20 \mu\text{inch } R_a$) and high roughness ($265.08 \mu\text{inch } R_a$) obtained from the PolyJet-printed airfoil measurements in the flow direction were selected for high velocity analysis. Moreover, flow analyses were conducted for all range of velocities using smooth and high roughness inputs to elucidate the effect of surface roughness for different velocities.

3. Results

3.1. Production and Surface Roughness Results

Figure 5 shows all the specimens produced after removing support structures. As seen, vertically oriented parts showed a very high amount of distortions especially in their trailing edges due to the small size of the trailing edge and slenderness. Furthermore, very high surface irregularities were observed on the side walls of vertically oriented specimens. Moreover, no visual print problem was observed on horizontally oriented specimens.

All surface roughness measurements results are shown in Table 4. It is monitored that the high amount of surface roughness values was observed in vertically oriented samples (Specimens 1–4). For vertically oriented samples, when measurements were performed

along the Z axis, parallel to the build direction, a higher amount of surface roughness values were observed than values taken along the X or Y axes. This is due to the nature of layer-by-layer manufacturing and stair-stepping effect of PolyJet. Some deviation in surface roughness results was observed especially in vertically oriented samples due to the overall geometrical deviation and distortion of these samples.

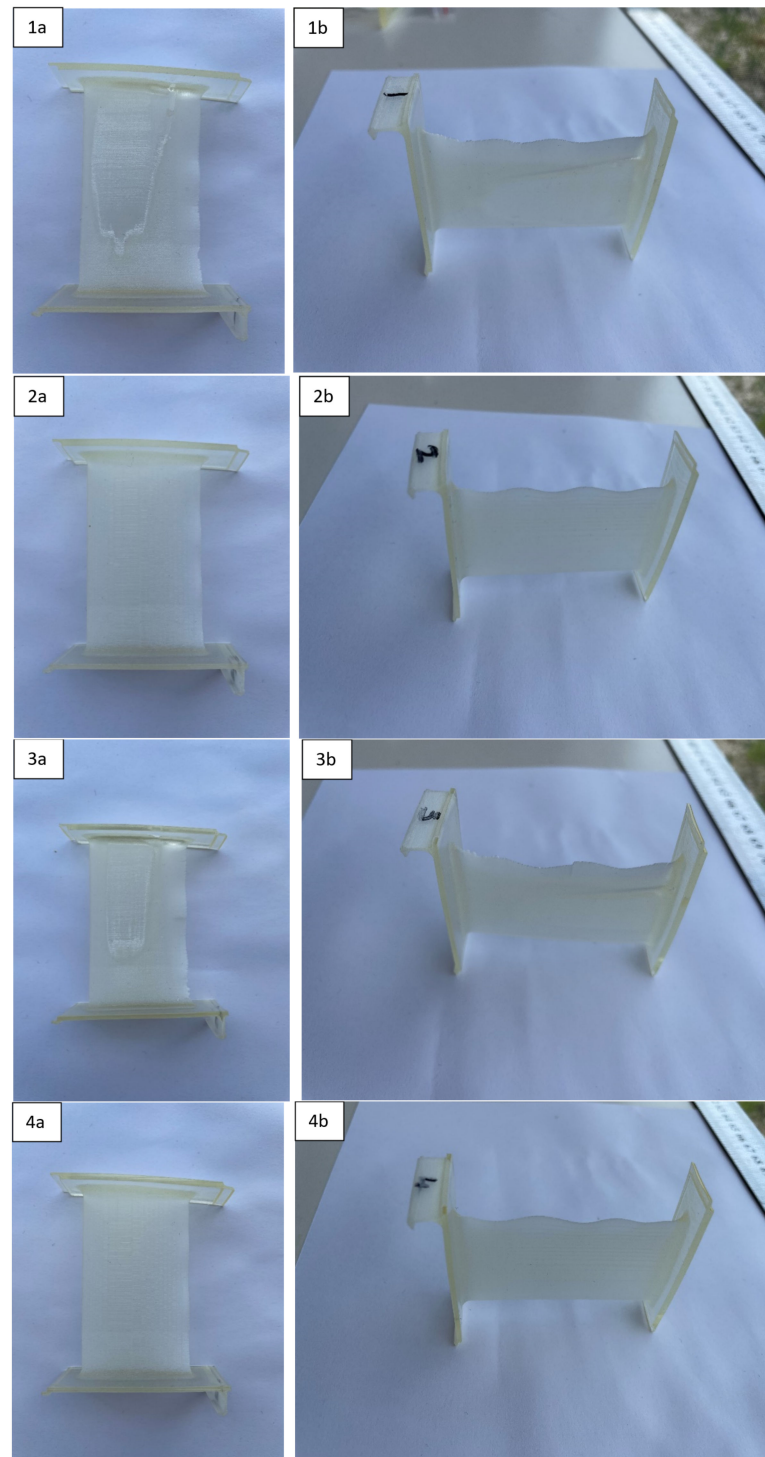


Figure 5. Cont.

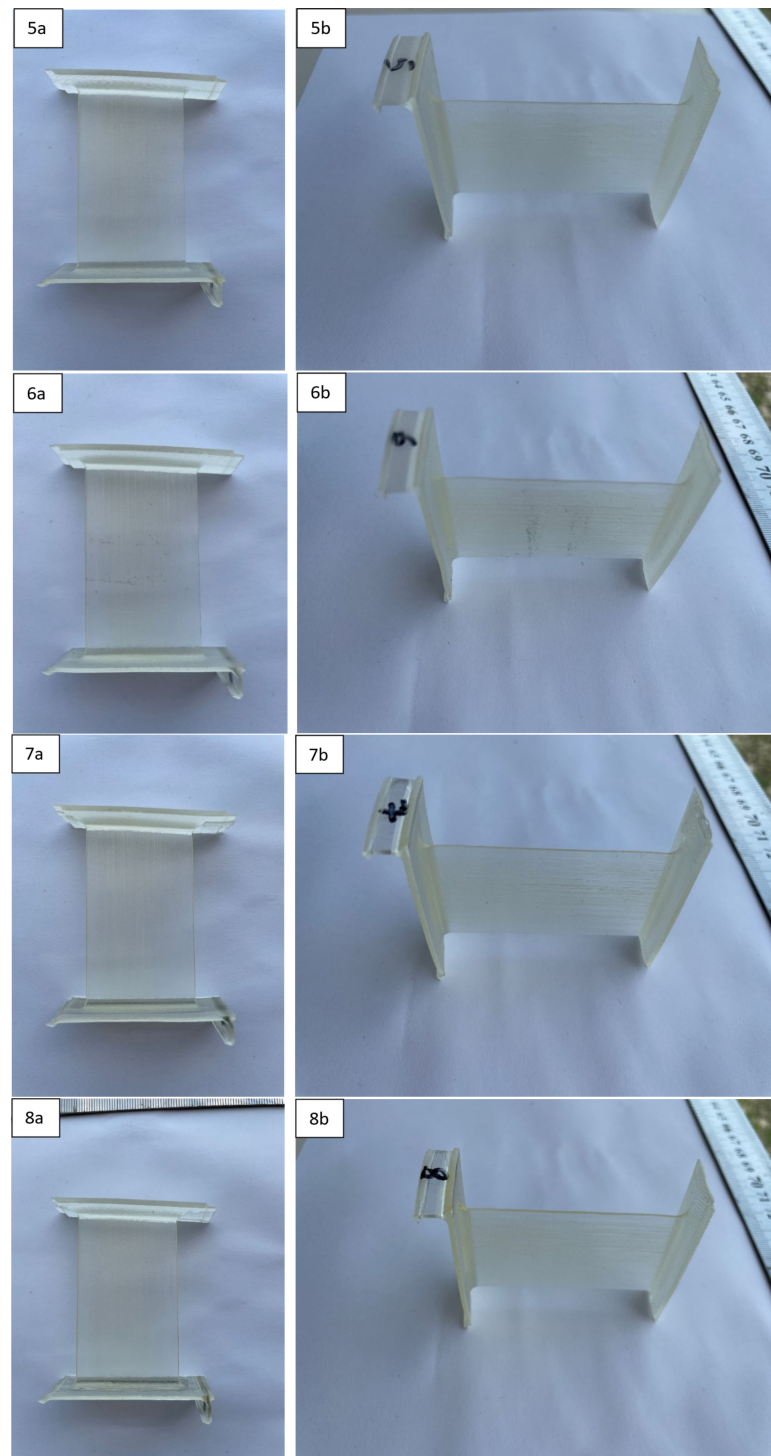


Figure 5. Printed specimens after support removal. Numbers at top left of the figures shows the related specimen.

3.2. Numerical Analysis Results

The estimation of the roughness effect on the drag and lift coefficients of the airfoil surfaces under different inlet velocities were performed using ANSYS Fluent[®] software, and drag and lift coefficients were captured as an output. Three different velocities were applied as inlet velocities: 40, 65 and 90 km/h for demonstrating the low-, moderate- and high-velocity UAVs. Arithmetical mean deviation (R_a) values that represent the surface roughness profile utilized in the analyses were obtained from the surface roughness mea-

measurements of PolyJet-printed polymer airfoil geometries (NACA0008) and were used as a roughness height input. In addition, analysis was conducted in all levels of velocities for smooth surfaces that had no surface roughness to put forward the effect of surface roughness by comparing the results as seen in Table 5. Furthermore, lift and drag coefficients were captured in different angles of attack ranging from -5° to 30° for smooth, mid-level and highest roughness under the highest inlet velocity of 90 km/h. Thus, the effect of the surface roughness on lift and drag coefficients resulting in a high velocity level (90 km/h inlet velocity) is demonstrated in Figures 6 and 7, respectively, to elucidate the best printing strategy for UAV wings for the purpose of providing better performance in different angles of attack. Additionally, lift and drag coefficient results for different surface roughness and angles of attack are compared to smooth surface results and displayed in Table 6. Furthermore, results show that the sensitivity of the lift coefficient to surface roughness profiles is more effective in comparison to the drag coefficient. In Table 5, drag and lift coefficients for smooth surfaces at different velocities are displayed, and the increase in velocity from low- to mid-level increases drag and lift coefficient by about 2.25- and 2.45-fold, respectively. However, an increase in velocity from mid-level to high for smooth surfaces increases drag and lift coefficient by about 1.75- and 1.85-fold, respectively. When the same analysis for smooth surfaces was performed for the highest surface roughness value, results show that the increase in drag coefficient by the increase in velocity does not change the increase rate considerably. However, an almost 10% increase rate is monitored in the lift coefficient. Besides, in comparison to the smooth surface, the highest surface roughness obtained from PolyJet printing generates a 7.5% difference in the drag and a 20% difference in the lift coefficient. As for different velocities, mid-level velocity generates an almost 4% increase in the drag and a 19% increase in the lift coefficient. For the low-velocity analysis, the effect of surface roughness on drag coefficient is 1.26%, and 10% for lift coefficient.

Figure 6 shows the lift coefficient variation in accordance with the angle of attack for three different roughness size models (smooth, mid-level and high roughness). Due to the symmetrical shape of NACA0008 airfoil, the lift coefficient experiences the least value at 0° angle of attack. Similar experimental results are seen for NACA0012 due to its symmetrical profile [56]. The pattern of curves shows that the increase in the angle of attack increases the lift coefficient gradually until reaching the maximum value, and a sudden drop is seen. The reduction in lift or so-called stalling phenomena is an undesirable issue for UAVs and aircrafts, and causes unsteady flight behavior. Thus, the results after stalling commences are not considered. Furthermore, the comparison of smooth mid-level roughness and smooth high roughness models show that the difference increases suddenly at a 10° angle of attack, in which the beginning of the stall region is experienced. Moreover, it is seen that the increase in surface roughness is highly effective in lift coefficient for a 0° angle of attack. Figure 7 displays the variation in the drag coefficient in accordance with the angle of attack for three different roughness models (smooth, mid-level and high roughness). The drag coefficient is minimal at 0° angle of attack due to symmetrical airfoil. It is seen that the increase in angle of attack directly increases the drag coefficient gradually until the maximum angle of attack. The increase in surface roughness increases the drag coefficient in all angle of attack degrees which is an undesirable issue that increases the energy consumption during the flight. The highest drag increase due to surface roughness is seen at a 10° angle of attack in which the beginning of the stall region is experienced.

Table 4. Surface roughness (R_a is in μinch) measurement results.

Specimen #	Measurement Directions Along	Measurement #	1st Surface *	1st Surface *	2nd Surface *	2nd Surface *
1	Y and Z	1st	59.6	16.6	341.7	477.1
		2nd	46.9	554.0	255.1	408.3
		3rd	10.6	687.9	200.6	369.3
		Average	39.03	419.5	265.8	418.23
2	X and Z	1st	35.9	248.7	51.7	377.3
		2nd	33.7	269.9	50.8	290.7
		3rd	32.5	289	63.4	398.4
		Average	34.0	269.2	55.3	355.5
3	Y and Z	1st	69.2	324.3	243.3	550.9
		2nd	52	387.5	148.5	506.7
		3rd	37.1	340.5	227.1	547.7
		Average	52.8	350.8	206.3	535.1
4	X and Z	1st	40.8	208.8	101.5	336.2
		2nd	44.8	230.7	90.1	323.2
		3rd	53.4	221	73.1	284.2
		Average	46.3	220.2	88.2	314.5
5	X and Y	1st	9.1	19.6	41.5	54.0
		2nd	9.3	14.5	33.2	59.0
		3rd	10.7	20.5	34.1	89.0
		Average	9.7	18.2	36.27	67.33
6	X and Y	1st	1.9	23.0	20.3	57.2
		2nd	1.1	23.8	22.6	48.2
		3rd	1.0	18.9	11.2	70.4
		Average	1.3	21.9	18.0	58.6
7	X and Y	1st	0.8	15.5	31.6	48.6
		2nd	10.2	14.5	59.1	52.3
		3rd	0.8	15.6	35.6	75.6
		Average	3.9	15.2	42.1	58.8
8	X and Y	1st	5.3	24.5	61.7	74.6
		2nd	7.7	21.7	43.8	55.4
		3rd	6.7	22.6	48.0	26.1
		Average	6.6	22.9	51.2	52.0

* # symbol represents number. For Specimens 1–4, the 1st surface is the surface closer to the left-hand side of build platform and the 2nd surface is the opposite surface. For Specimens 5–8, the 1st surface is up-facing, and the 2nd surface is down-facing surfaces. Measurements on Columns 4 and 6 are along the first direction stated in Column 2. Measurements on Columns 5 and 7 are along the second direction stated in Column 2.

Table 5. Surface roughness effect on C_L and C_D values for different velocities at 0° angle of attack.

Velocity	R_a Value (μinch)	C_D	C_D Diff. (%)	C_L	C_L Diff. (%)
90 km/h	0	1.43×10^{-4}	-	1.24×10^{-4}	-
	265.08	1.54×10^{-4}	7.48	9.83×10^{-5}	-20.66
65 km/h	0	8.21×10^{-5}	-	6.371×10^{-5}	-
	265.08	8.52×10^{-5}	3.71	5.358×10^{-5}	-18.90
40 km/h	0	3.67×10^{-5}	-	2.403×10^{-5}	-
	265.08	3.72×10^{-5}	1.26	2.199×10^{-5}	-9.29

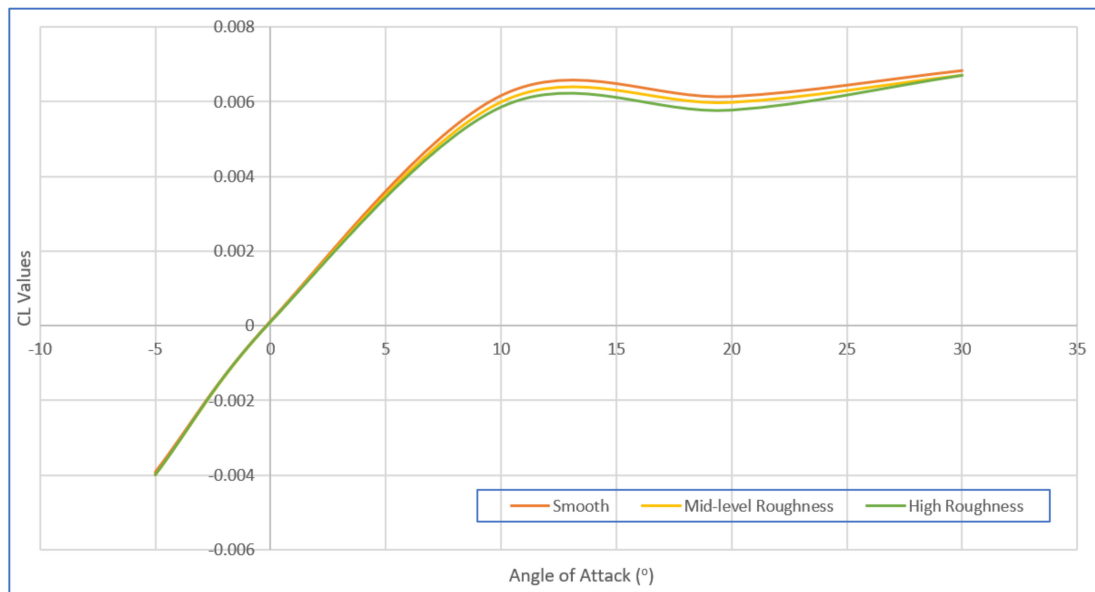


Figure 6. Surface roughness effect on C_L values for 90 km/h inlet velocity.

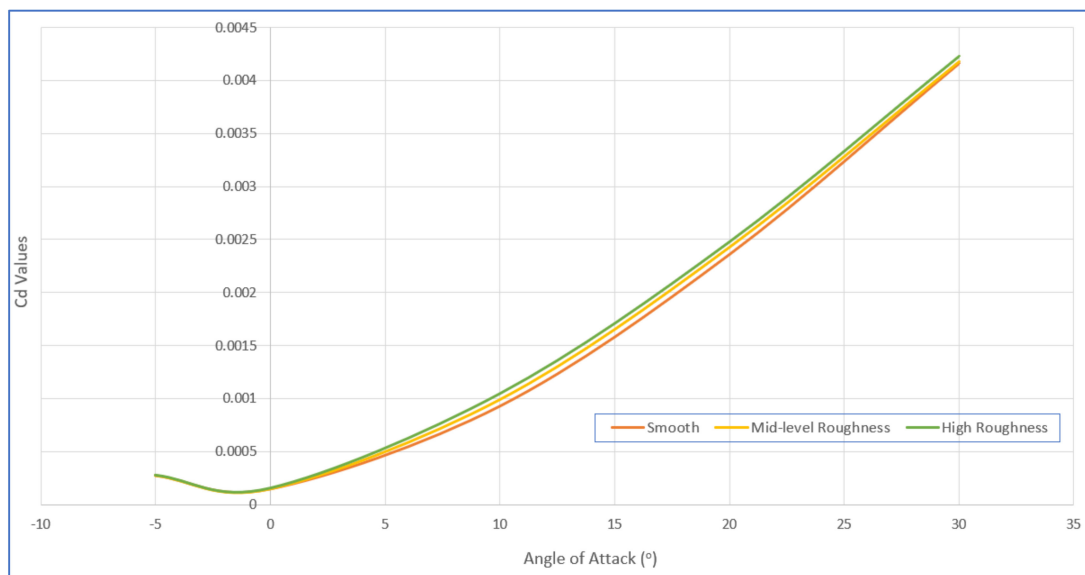


Figure 7. Surface roughness effect on C_D values for 90 km/h inlet velocity.

Table 6. Surface roughness effect on C_L and C_D values for 90 km/h inlet velocity.

Angle of Attack ($^\circ$)	Ra Value (μ inch)	C_D	C_D Diff. with Smooth (%)	C_L	C_L Diff. with Smooth (%)
−5	0	2.70×10^{-4}		-3.92×10^{-3}	
	88.20	2.73×10^{-4}	1.18	-3.99×10^{-3}	1.74
	265.08	2.76×10^{-4}	2.37	-4.00×10^{-3}	1.83
0	0	1.43×10^{-4}		1.24×10^{-4}	
	88.20	1.47×10^{-4}	2.89	1.07×10^{-4}	−13.65
	265.08	1.54×10^{-4}	7.48	9.83×10^{-5}	−20.66
5	0	2.42×10^{-4}		3.94×10^{-3}	
	88.20	2.45×10^{-4}	1.02	3.91×10^{-3}	−0.75
	265.08	2.46×10^{-4}	1.32	3.89×10^{-3}	−1.13
10	0	9.25×10^{-4}		6.16×10^{-3}	
	88.20	9.88×10^{-4}	6.81	6.00×10^{-3}	−2.66
	265.08	1.05×10^{-3}	12.96	5.85×10^{-3}	−5.10
15	0	1.63×10^{-3}		5.39×10^{-3}	
	88.20	1.64×10^{-3}	1.06	5.33×10^{-3}	−1.06
	265.08	1.67×10^{-3}	2.47	5.29×10^{-3}	−1.79
20	0	2.36×10^{-3}		6.14×10^{-3}	
	88.20	2.42×10^{-3}	2.79	5.99×10^{-3}	−2.43
	265.08	2.48×10^{-3}	5.10	5.77×10^{-3}	−6.04
25	0	3.20×10^{-3}		6.78×10^{-3}	
	88.20	3.32×10^{-3}	3.65	6.54×10^{-3}	−3.63
	265.08	3.44×10^{-3}	7.40	6.26×10^{-3}	−7.69
30	0	4.16×10^{-3}		6.83×10^{-3}	
	88.20	4.17×10^{-3}	0.26	6.72×10^{-3}	−1.69
	265.08	4.23×10^{-3}	1.66	6.70×10^{-3}	−1.98

4. Discussion

Figure 8 shows surface roughness measurements on both surfaces of all specimens, and it is clear that surface roughness measurements along Z direction for Specimens 1–4 are higher than measurements along X or Y direction due to layer-by-layer manufacturing and stair-stepping effect. For Specimens 5–8, surface roughness measurements along the X direction are lower than along the Y direction. For Specimens 1–4, surface roughness values on the 1st surfaces are higher than that on 2nd surfaces and for Specimens 5–8, it can be seen from Figure 8 that up-facing surfaces have lower surface roughness values than down-facing surfaces due to the fact that up-facing surfaces are naturally supported by previous layers of the same material, but down-facing surfaces have support of different materials (SUP706B). For all specimens and surfaces, the lowest surface roughness value was observed on the up-facing surface of specimen 6 where the specimen was located along X axis and horizontal build orientation and matte surface setting were used, and measurement was performed along the X direction. On the other hand, the highest surface roughness was observed on the 2nd surface of specimen 3 where the specimen was located along the Y axis and a vertical build orientation and glossy surface setting were used, and measurement was performed along Z direction.

4.1. Effect of Tray Location of Specimens on Surface Roughness

Figure 8 reveals that, when build orientation and surface finish settings are the same, printing along the X direction, in general, resulted in parts with lower surface roughness than parts printed along the Y direction (comparison between part pairs 1–2, 3–4, 5–6 and 7–8) for all surfaces with a small amount of difference. As stated by Barclift et al., the distribution of the same parts on the build platform can affect mechanical properties

due to the over-curing of some parts in different locations while other parts are being cured. They also stated that decreasing the parts' spacing increased the parts' strength [57]. Pilipović et al., stated that accuracy and repeatability in the X and Y axis is better than it is for the Z axis based on distance measurements in PolyJet technology [11]. Cazon et al., stated that parts printed along the X axis gave the best results in terms of stiffness [15]. According to the results of the present study and the available literature, it can be suggested that for better surface quality and strength, airfoil geometries need to be oriented along the X axis when printed in PolyJet.

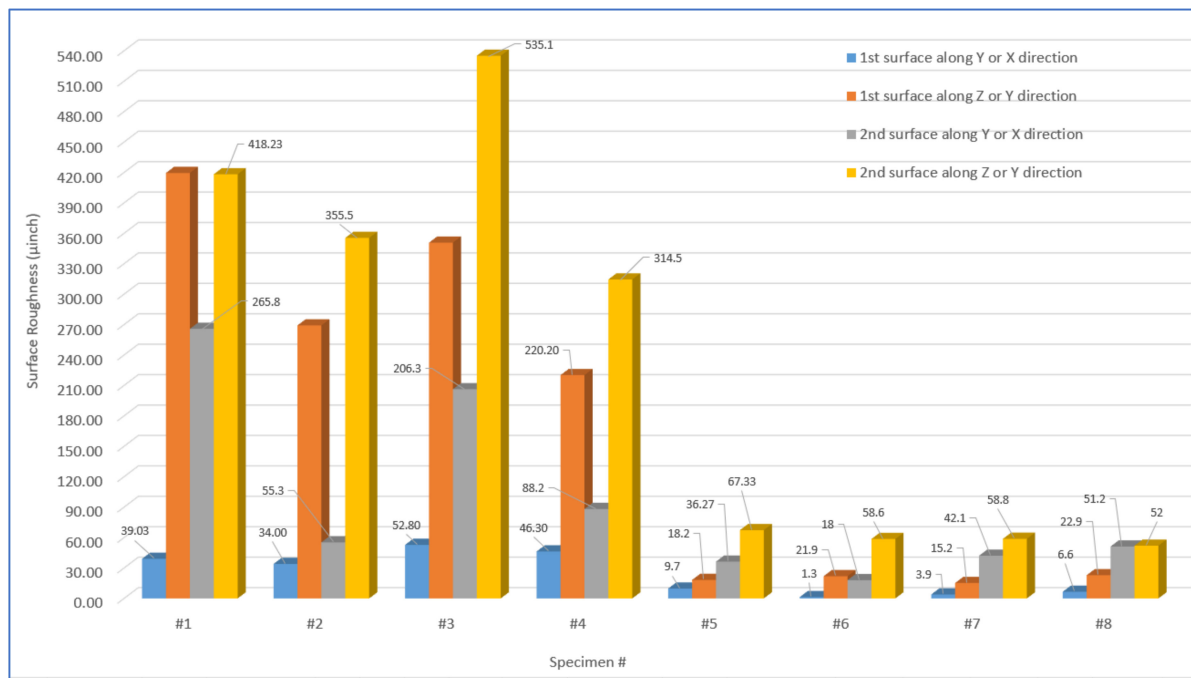


Figure 8. Surface roughness measurements results on both surfaces of all specimens.

4.2. Effect of Build Orientation on Surface Roughness

It can be seen from Figure 8 that when tray location and surface finish settings are the same, horizontal build orientation resulted in parts with lower surface roughness than vertical build orientation (comparison between part pairs 1–5, 2–6, 3–8 and 4–7) for all surfaces. These results have good consistency with the available literature [19–23]. Since vertically built specimens have a high amount of distortion, especially at trailing edges, and higher surface roughness values, it can be suggested that for better surface quality and lower distortion, airfoil geometries need to be horizontally built in PolyJet.

4.3. Effect of Surface Finish Setting on Surface Roughness

As stated before, in the matte setting, the whole part is covered with support material, and in the glossy setting, only structurally needed areas are supported. For this reason, it is more meaningful to see the effect of surface finish setting on surface roughness for up-facing surfaces of Specimens 5–8. Based on the comparison between surface roughness measurements on 1st surfaces (up-facing surfaces) of part pairs 5–8 and 6–7 where tray locations and build orientations were the same and only surface finish settings were changed, it can be stated that, in general, the glossy surface finish setting showed better surface quality than the matte surface finish setting with a small difference, but it is also clear that this situation depends on location of the specimen on build plate. Therefore, it can generally be suggested that for better surface quality, airfoil geometries need to be built with the glossy surface finish option in PolyJet.

4.4. Effect of Surface Roughness on Flight Performance

It can be seen that build strategy and, because of this, the surface roughness of the PolyJet-printed parts directly influence the aerodynamic performance of fixed-wing UAVs. For high-velocity UAVs, the effect of surface roughness arithmetic deviation on drag and lift coefficients reaches a difference of 7.5% and -20% , respectively, in comparison to the smooth-surfaced airfoils. Furthermore, the drag force is the movement resistance of an object in a fluid environment; thus, the increase in drag coefficient directly increases the power needed to maintain cruise in the air. Furthermore, lift force is a force that is exerted by the surrounded fluid in the perpendicular direction of the oncoming flow direction, and it counters the force of gravity; thus, the floating in the fluid is provided [41]. Therefore, any reduction in the lift coefficient due to surface roughness needs to be compensated by the increase of the UAV's velocity. Hereby, additional power is needed to avoid a decrease in cruise distance. According to the results, the effect of surface roughness on drag and lift coefficients approaches the values of 3.71% and -18.90% for mid-velocities and 1.26% and -9.29% for low velocities, respectively. Besides, the effect of surface roughness values changes highly according to different angles of attack; 0° and 10° attack angles are the critical angles at which lift and drag coefficient, respectively, are highly affected. Consequently, the print configuration that is used for the production of the specimen 5, which includes a Y axis tray location, horizontal build orientation and matte surface finish setting, is the best option for aerodynamic performance in terms of surface roughness with the least surface roughness in the flow direction.

5. Conclusions

The experimental part of study focused on the effect of tray location, build direction and surface finish options on surface roughness values of airfoil geometries printed in PolyJet. Two sides of airfoil surfaces were measured along two crossing directions. The numerical part is focused on the aerodynamic performance of PolyJet-printed parts in terms of different surface roughness profiles in the flow direction, velocities and angles of attack. The following findings can be drawn from this study:

- Airfoil geometries located along X direction have lower surface roughness values than geometries located along Y direction. Therefore, it is suggested to print airfoil geometries along X direction for better surface quality;
- Airfoil geometries with vertical build orientation have very high distortion especially on trailing edge areas and higher surface roughness values than geometries with horizontal build orientation. Therefore, it is suggested to print airfoil geometries with horizontal build orientation for lower distortion and better surface quality;
- It was observed that matte and glossy surface finish settings resulted in different surface roughness values in different surfaces, and it is very difficult to make a correlation between surface finish settings and surface roughness. However, in general, it can be suggested to print airfoil geometries with glossy surface finish setting for better surface quality.
- Surface roughness of the PolyJet-printed fixed-wing UAV wings affects the drag coefficient 7.5% in high velocity cruises. Thus, convenient build orientations should be selected to reduce the surface roughness for increasing the aerodynamic performance. By this, the limited cruise distance of UAVs can be increased. Thus, it is suggested that the build configuration of including Y axis tray location, horizontal build orientation and matte surface finish setting is the best option for aerodynamic performance in terms of surface roughness with the least surface roughness in the flow direction.

Author Contributions: Conceptualization, O.G. and K.G.; methodology, O.G. and K.G.; software, K.G.; validation, O.G., A.Ç. and K.G.; investigation, O.G. and K.G.; resources, O.G. and K.G.; data curation, A.Ç.; writing—original draft preparation, O.G. and K.G.; writing—review and editing, O.G., K.G. and A.Ç.; visualization, O.G., A.Ç. and K.G. All authors have read and agreed to the published version of the manuscript.

Funding: This research was funded by Technological and Scientific Council of Turkey (TUBITAK) Technology and Innovation Support Program grant number 5158001.

Institutional Review Board Statement: Not applicable.

Informed Consent Statement: Not applicable.

Data Availability Statement: The data presented in this study are available on request from the corresponding author.

Conflicts of Interest: The authors declare no conflict of interest. The funders had no role in the design of the study; in the collection, analyses, or interpretation of data; in the writing of the manuscript, or in the decision to publish the results.

References

1. Gupta, S.G.; Ghonge, M.M.; Jawandhiya, P.M. Review of unmanned aircraft system (UAS). *Int. J. Adv. Res. Comp. Eng. Technol.* **2013**, *2*, 1646–1658. [[CrossRef](#)]
2. Shakhathreh, H.; Sawalmeh, A.H.; Al-Fuqaha, A.; Dou, Z.; Almaita, E.; Khalil, I.; Othman, N.S.; Khreishah, A.; Guizani, M. Unmanned aerial vehicles (UAVs): A survey on civil applications and key research challenges. *IEEE Access* **2019**, *7*, 48572–48634. [[CrossRef](#)]
3. Rahman, M.F.F.; Fan, S.; Zhang, Y.; Chen, L. A comparative study on application of unmanned aerial vehicle systems in agriculture. *Agriculture* **2021**, *11*, 22. [[CrossRef](#)]
4. Giordan, D.; Adams, M.S.; Aicardi, I.; Alicandro, M.; Allasia, P.; Baldo, M.; De Berardinis, P.; Dominici, D.; Godone, D.; Hobbs, P.; et al. The use of unmanned aerial vehicles (UAVs) for engineering geology applications. *Bull. Eng. Geol. Environ.* **2020**, *79*, 3437–3481. [[CrossRef](#)]
5. PS, R.; Jeyan, M.L. Mini unmanned aerial systems (UAV)—A review of the parameters for classification of a mini UAV. *Int. J. Aviat. Aeronaut. Aerosp.* **2020**, *7*, 5. [[CrossRef](#)]
6. Hassanalian, M.; Abdelkefi, A. Classifications, applications, and design challenges of drones: A review. *Prog. Aerosp. Sci.* **2017**, *91*, 99–131. [[CrossRef](#)]
7. Herzog, D.; Seyda, V.; Wycisk, E.; Emmelmann, C. Additive manufacturing of metals. *Acta Mater.* **2016**, *117*, 371–392. [[CrossRef](#)]
8. Najmon, J.C.; Raeksi, S.; Tovar, A. Review of additive manufacturing technologies and applications in the aerospace industry. In *Additive Manufacturing for the Aerospace Industry*; Froes, F., Boyer, R., Eds.; Elsevier: Amsterdam, The Netherlands, 2019; pp. 7–31.
9. Gülcan, O.; Günaydin, K.; Tamer, A. The state of the art of material jetting—A critical review. *Polymers* **2021**, *13*, 2829. [[CrossRef](#)]
10. Leary, M. *Design for Additive Manufacturing*; Elsevier: Amsterdam, The Netherlands, 2020; p. 270.
11. Pilipović, A.; Baršić, G.; Katić, M.; Havstad, M.R. Repeatability and reproducibility assessment of a PolyJet technology using x-ray computed tomography. *Appl. Sci.* **2020**, *10*, 7040. [[CrossRef](#)]
12. Gardan, J. Additive manufacturing technologies: State of the art and trends. *Int. J. Prod. Res.* **2016**, *54*, 3118–3132. [[CrossRef](#)]
13. O’Neill, P.; Jolivet, L.; Kent, N.J.; Brabazon, D. Physical integrity of 3D printed parts for use as embossing tools. *Adv. Mater. Process. Technol.* **2017**, *3*, 308–317. [[CrossRef](#)]
14. Stansbury, J.W.; Idacavage, M.J. 3D printing with polymers: Challenges among expanding options and opportunities. *Dent. Mater.* **2016**, *32*, 54–64. [[CrossRef](#)] [[PubMed](#)]
15. Cazón, A.; Morer, P.; Matey, L. PolyJet technology for product prototyping: Tensile strength and surface roughness properties. *Proc. Inst. Mech. Eng. Part B J. Eng. Manuf.* **2014**, *228*, 1664–1675. [[CrossRef](#)]
16. Kechagias, J.; Iakovakis, V.; Giorgo, E.; Stavropoulos, P.; Koutsomichalis, A.; Vaxevanidis, N.M. Surface roughness optimization of prototypes produced by PolyJet direct 3d printing technology. In Proceedings of the International Conference on Engineering and Applied Sciences Optimization, Kos Island, Greece, 4–6 June 2014.
17. Aslani, K.; Vakouftsi, F.; Kechagias, J.D.; Mastorakis, N.E. Surface roughness optimization of Poly-Jet 3D printing using grey taguchi method. In Proceedings of the International Conference on Control Artificial Intelligence, Robotics & Optimization (ICCAIRO), Athens, Greece, 3–5 May 2019; pp. 213–218.
18. Beltrán, N.; Carriles, F.; Álvarez, B.J.; Blanco, D.; Rico, J.C. Characterization of factors influencing dimensional and geometric errors in PolyJet manufacturing of cylindrical features. *Procedia Eng.* **2015**, *132*, 62–69. [[CrossRef](#)]
19. Kumar, K.; Kumar, G.S. A study on surface roughness of rapid prototypes fabricated using PolyJet 3D printing system. In Proceedings of the International Conference on Computer Aided Engineering (CAE 2013), Madras, India, 19–21 December 2012; pp. 1–6.
20. Kumar, K.; Kumar, G.S. An experimental and theoretical investigation of surface roughness of poly-jet printed parts. *Virtual Phys. Prototyp.* **2015**, *10*, 23–34. [[CrossRef](#)]
21. Kechagias, J.; Stavropoulos, P. An investigation of sloped surface roughness of direct poly-jet 3D printing. In Proceedings of the International Conference on Industrial Engineering-INDE, Zakynthos Island, Greece, 16–20 July 2015; pp. 150–153.
22. Khoshkhoo, A.; Carrano, A.L.; Blerch, D.M. Effect of surface slope and build orientation on surface finish and dimensional accuracy in material jetting processes. *Procedia Manuf.* **2018**, *26*, 720–730. [[CrossRef](#)]

23. Vidakis, N.; Petousis, M.; Vaxevanidis, N.; Kechagias, J. Surface roughness investigation of Poly-Jet 3D printing. *Mathematics* **2020**, *8*, 1758. [CrossRef]
24. Kent, N.J.; Jolivet, L.; O'Neill, P.; Brabazon, D. An evaluation of components manufactured from a range of materials, fabricated using PolyJet technology. *Adv. Mater. Process. Technol.* **2017**, *3*, 318–329. [CrossRef]
25. Matte or Glossy? Which Finish to Use for Your 3D Prints and When. Available online: <https://grabcad.com/tutorials/matte-or-glossy-which-finish-to-use-for-your-3d-prints-and-when> (accessed on 13 September 2021).
26. Pugalendhi, A.; Ranganathan, R.; Chandrasekaran, M. Effect of process parameters on mechanical properties of VeroBlue material and their optimal selection in PolyJet technology. *Int. J. Adv. Manuf. Technol.* **2020**, *108*, 1049–1059. [CrossRef]
27. Moore, J.P.; Williams, C.B. Fatigue properties of parts printed by PolyJet material jetting. *Rapid Prototyp. J.* **2015**, *21*, 675–685. [CrossRef]
28. Ferro, C.; Grassi, R.; Secli, C.; Maggiore, P. Additive manufacturing offers new opportunities in UAV research. *Procedia CIRP* **2016**, *41*, 1004–1010. [CrossRef]
29. Kim, S.-Y.; Shin, Y.-S.; Jung, H.-D.; Hwang, C.-J.; Baik, H.-S.; Cha, J.-Y. Precision and trueness of dental models manufactured with different 3-dimensional printing techniques. *Am. J. Orthod. Dentofac. Orthop.* **2018**, *153*, 144–153. [CrossRef] [PubMed]
30. Maurya, N.K.; Rastogi, V.; Singh, P. Comparative study and measurement of form errors for the component printed by FDM and polyjet process. *Instrum. Mes. Métrologie* **2019**, *18*, 353–359. [CrossRef]
31. Dizon, J.R.C.; Valino, A.D.; Souza, L.R.; Espera, A.H.; Chen, Q.; Advincula, R.C. 3D printed injection molds using various 3D printing technologies. *Mater. Sci. Forum* **2020**, *1005*, 150–156. [CrossRef]
32. Lee, K.Y.; Cho, J.W.; Chang, N.Y.; Chae, J.M.; Kang, K.H.; Kim, S.C.; Cho, J.H. Accuracy of three-dimensional printing for manufacturing replica teeth. *Korean J. Orthod.* **2015**, *45*, 217–225. [CrossRef]
33. Hosseiniabadi, H.G.; Bagheri, R.; Gray, L.A.; Altstädt, V.; Drechsler, K. Plasticity in polymeric honeycombs made by photopolymerization and nozzle based 3D-printing. *Polym. Test.* **2017**, *63*, 163–167. [CrossRef]
34. Li, Y.; Linke, B.S.; Voet, H.; Falk, B.; Schmitt, R.; Lam, M. Cost, sustainability and surface roughness quality—A comprehensive analysis of products made with personal 3D printers. *CIRP J. Manuf. Sci. Technol.* **2017**, *16*, 1–11. [CrossRef]
35. Queral, V.; Rincón, E.; Mirones, V.; Rios, L.; Cabrera, S. Dimensional accuracy of additively manufactured structures for modular coil windings of stellarators. *Fusion Eng. Des.* **2017**, *124*, 173–178. [CrossRef]
36. Tan, W.S.; Suwarno, S.R.; An, J.; Chua, C.K.; Fane, A.G.; Chong, T.H. Comparison of solid, liquid and powder forms of 3D printing techniques in membrane spacer fabrication. *J. Membr. Sci.* **2017**, *537*, 283–296. [CrossRef]
37. Budzik, G.; Woźniak, J.; Paszkiewicz, A.; Przeszlowski, L.; Dziubek, T.; Dębski, M. Methodology for the quality control process of additive manufacturing products made of polymer materials. *Materials* **2021**, *14*, 2202. [CrossRef]
38. Goh, G.D.; Agarwala, S.; Goh, G.L.; Dikshit, V.; Yeong, W.Y. Additive manufacturing in unmanned aerial vehicles (UAVs): Challenges and potential. *Aerosp. Sci. Technol.* **2017**, *63*, 140–151. [CrossRef]
39. Villa, T.F.; Gonzalez, F.; Miljievic, B.; Ristovski, Z.D.; Morawska, L. An overview of small unmanned aerial vehicles for air quality measurements: Present applications and future perspectives. *Sensors* **2016**, *16*, 1072. [CrossRef] [PubMed]
40. Tamila, Y. Using the ANSYS Workbench software for designing of the miniature unmanned aerial vehicles. Proceedings of Computer Science & Engineering, Lviv, Ukraine, 21–23 November 2013.
41. Anderson, J.D., Jr. *Fundamentals of Aerodynamics*; Tata McGraw-Hill Education: New York, NY, USA, 2010; ISBN 0070700125.
42. Carmichael, B.H. *Low Reynolds Number Airfoil Survey*; NASA Report No. 165803; NASA: Washington, DC, USA, 1981.
43. Eisenbeiss, H. A mini unmanned aerial vehicle (UAV): System overview and image acquisition. *Int. Arch. Photogramm. Remote Sens. Spat. Inf. Sci.* **2004**, *36*, 1–7.
44. Chmielewski, P.; Sibilski, K. Ground Speed Optical Estimator for Miniature UAV. *Sensors* **2021**, *21*, 2754. [CrossRef] [PubMed]
45. Mittal, P.; Muneshwar, R.N. Market analysis and potential of uav systems for monitoring & cartography in ecology, agriculture & forestry. *Sci. Youth* **2012**, *11–12*, 135–137.
46. Ni, D.; Yu, G.; Rathinam, S. Unmanned aircraft system and its applications in transportation. *J. Adv. Transport.* **2017**, *2017*, 7156153. [CrossRef]
47. Xiaoyu, S.; Zhenyu, G.; Ruizhi, M.; Jie, L.; Chengwei, Y. Reinforcement-learning-based miniature UAV identification. In Proceedings of the IEEE International Conference on Unmanned Systems (ICUS), Beijing, China, 27–29 October 2017; pp. 237–242.
48. Dündar, Ö.; Bilici, M.; Ünler, T. Design and performance analyses of a fixed wing battery VTOL UAV. *Eng. Sci. Technol. Int. J.* **2020**, *23*, 1182–1193. [CrossRef]
49. Fluent, A. *Fluent 14.0 User's Guide*; ANSYS FLUENT Inc.: Lebanon, NH, USA, 2011.
50. Sadikin, A.; Yunus, N.A.M.; Abd Hamid, S.A.; Md Salleh, S.; Rahman, M.N.A.; Mahzan, S.; Ayop, S.S. A comparative study of turbulence models on aerodynamics characteristics of a NACA0012 airfoil. *Int. J. Integ. Eng.* **2018**, *1*, 10. [CrossRef]
51. Versteeg, H.; Malalasekera, W. *An Introduction to Computational Fluid Dynamics: The Finite Volume Method*; Pearson Education: London, UK, 2007; ISBN 0131274988.
52. Pang, A.L.J.; Skote, M.; Lim, S.Y. Modelling high Re flow around a 2D cylindrical bluff body using the k- ω (SST) turbulence model. *Prog. Comput. Fluid Dyn. Int. J.* **2016**, *16*, 48–57. [CrossRef]
53. Bons, J.P. A review of surface roughness effects in gas turbines. *ASME J. Turbomach.* **2010**, *132*, 021004. [CrossRef]
54. Pattanapol, W.; Wakes, S.J.; Hilton, M.J.; Dickinson, K.J.M. Modeling of surface roughness for flow over a complex vegetated surface. *Int. J. Math. Phys. Eng. Sci.* **2008**, *2*, 18–26.

-
55. Adams, T.; Grant, C.; Watson, H. A simple algorithm to relate measured surface roughness to equivalent sand-grain roughness. *Int. J. Mech. Eng. Mechatron.* **2012**, *1*, 66–71. [[CrossRef](#)]
 56. Chakroun, W.; Al-Mesri, I.; Al-Fahad, S. Effect of surface roughness on the aerodynamic characteristics of a symmetrical airfoil. *Wind Eng.* **2004**, *28*, 547–564. [[CrossRef](#)]
 57. Hummel, F.; Lötzerich, M.; Cardamone, P.; Fottner, L. Surface roughness effects on turbine blade aerodynamics. *ASME J. Turbomach.* **2005**, *127*, 453–461. [[CrossRef](#)]